Applied Catalysis B: Environmental 180 (2016) 130–138

Contents lists available at ScienceDirect

Applied Catalysis B: Environmental

journal homepage: www.elsevier.com/locate/apcatb

Ag-loading on brookite TiO_2 quasi nanocubes with exposed {2 1 0} and {0 0 1} facets: Activity and selectivity of CO_2 photoreduction to CO/CH_4

Kan Li, Tianyou Peng*, Zihao Ying, Shuaishuai Song, Jing Zhang

College of Chemistry and Molecular Science, Wuhan University, Wuhan 430072, PR China

ARTICLE INFO

Article history:
Received 4 May 2015
Received in revised form 9 June 2015
Accepted 15 June 2015
Available online 19 June 2015

Keywords:
Brookite TiO_2
Exposed facet
Ag-loading
CO_2 photoreduction
Selectivity

ABSTRACT

Brookite TiO_2 quasi nanocubes (mean size of ~50 nm) mainly surrounded by four {2 1 0} and two {0 0 1} exposed crystal facets were used as catalyst for the CO_2 photoreduction. It is found that the Ag nanoparticle size and its distribution on the exposed facets of the brookite nanocubes are significantly influenced by the Ag-loading levels, which then causing obvious differences in the activity and selectivity of CO_2 photoreduction to CO/CH_4 generation. At 0.5% Ag-loading, the brookite nanocubes show the highest overall activity with CO/CH_4 production rates of 128.8/11.5 ppm h^{-1}, which is 3.89 times higher than that of the pristine brookite. When the Ag-loading level is ≤0.5%, the small Ag nanoparticles are mainly dispersed on the {2 1 0} facets of the brookite nanocubes, which resulting in an enhancement in the selective CO generation; while >0.5% Ag-loading could lead to the formation of Ag nanoparticles aggregated on the {2 1 0} facets with some Ag nanoparticles dispersed on the {0 0 1} facets, and then causing more selectivity for the CH_4 generation. This novel phenomenon was explored with the aid of various characterization techniques. The present results provide an important indication about the effects of Ag-loading on the activity and selectivity of CO_2 photoreduction reaction over the exposed facets of brookite nanocubes, and demonstrate a strategy for tuning the CO_2 photoreduction performance through tailoring the morphology and surface structure of brookite TiO_2.

1. Introduction

As a major greenhouse gas causing global warming, CO_2 level in the atmosphere has been increasing steadily over the past centuries as a result of human activities, and therefore the fixation and conversion of CO_2 into C1/C2 energy compounds (such as CO, CH_4, CH_3OH, and/or C_2H_5OH) becomes a global knowledge [1]. Since CO_2 conversion is an uphill reaction ($\Delta G > 0$), many strategies such as catalyzed chemical, thermochemical, electrochemical, photochemical, and photoelectrochemical CO_2 conversion have been developed by using various induced energy sources [2–4]. Among which, photocatalytic CO_2 reduction may be the most promising way since it can provide a package solution to the currently energy and environment problems by utilizing the inexhaustible solar energy to reduce the excessive CO_2 emission and produce marketable solar fuels at the same time [5–11].

Since CO_2 does not absorb either visible or UV radiation, CO_2 photoreduction is a process requiring suitable photocatalyst, such as metal oxide/sulfide [12–17], carbon nitride [18], carbon nanotubes [19], and graphene oxide [20], to absorb UV-vis light and transfer it to CO_2. Generally, CO_2 photoreduction over catalyst can be conducted in liquid or gaseous phase system [7–11]. Some liquid CO_2 photoreduction reactions were conducted in an alkaline solution, which leads to the difficulty to determine the initial reactant due to the ionization equilibrium among carbonate (CO_3^{2-}), bicarbonate (HCO_3^-) and carbon dioxide (CO_2 and H_2CO_3) [15,21]. Therefore, it is preferable to investigate the CO_2 photoreduction property in gaseous system, which ensures the reactants are CO_2 and H_2O vapor so as to investigate the critical influencing factors to the activity/selectivity by adjusting the gaseous CO_2/H_2O concentrations and the catalyst's microstructure [16–18,22–25].

Up till now, nanosized TiO_2 is the most extensively applied UV-light-driven catalyst in the CO_2 photoreduction system because of its high stability and durability with a low tendency to deactivation and/or corrosion [1–5]. Among the three TiO_2 polymorphs (anatase, brookite and rutile) that exist in nature, anatase, rutile and its mixed crystal have been comprehensively studied and applied

* Corresponding author.
E-mail address: typeng@whu.edu.cn (T. Peng).

http://dx.doi.org/10.1016/j.apcatb.2015.06.022
0926-3373/

in the fields of photocatalysis and photoelectric conversion [26,27], while brookite is rarely investigated due to the difficulty encountered in obtaining its pure phase [28–32]. Nevertheless, theoretical investigations have indicated that brookite should have better photocatalytic and/or photoelectrical properties than anatase and rutile [28,29], although high-quality brookite and its application have seldom been reported till now [30–33]. Moreover, Liu et al. [32] have found that helium pretreatment of TiO_2 resulted in the creation of surface oxygen vacancies (V_O) and Ti^{3+} sites on anatase and brookite but not on rutile, and the photocatalytic activity for the CO_2 photoreduction to CO/CH_4 were remarkably enhanced on the defective anatase and brookite (up to 10-fold enhancement) compared to the defect-free surfaces. The better activity of the defective brookite than anatase and rutile was ascribed to the lower formation energy of the V_O on brookite [32]. Recently, Lin et al. [30] have reported that high-quality brookite TiO_2 single-crystal nanosheets surrounded with four {2 1 0}, two {1 0 1}, and two {2 0 1} exposed facets exhibited outstanding activity for the organic contaminant degradation due to the exposure of high-energy crystal facets and the effective suppression of the charge recombination caused by these facets acting as the oxidative and reductive sites, respectively. Similarly, the CO_2 photoreduction activity of an exposed-crystal-facet-controlled brookite nanorods is depended on its aspect ratio because the {2 1 0} facets worked as reduction site, and Au or Ag on the reduction facets of the brookite nanorods can increase the CH_3OH generation [31]. The above investigations showed that brookite would have activity in the CO_2 photoreduction to solar fuels, which can be adjusted through proper microstructure and/or crystal facet modification.

More recently, brookite TiO_2 quasi nanocubes with high phase purity and a mean particle size of ~50 nm are synthesized through a hydrothermal method in our group [34]. The obtained brookite TiO_2 nanocubes are mainly surrounded by four {2 1 0} and two {0 0 1} exposed facets. By using the brookite nanocubes as overlayer of the nanosized anatase TiO_2 film, the corresponding bilayer solar cell with an optimized overlayer thickness gives photovoltaic conversion efficiency up to 8.83%, with 23.8% improvement as compared to the single anatase TiO_2-based cell (7.13%) [34]. Herein, Ag nanoparticles are loaded on those brookite TiO_2 nanocubes (denoted as Ag–TiO_2) through a traditional chemical reduction method. It is found that the Ag-loading on different exposed crystal facets of the brookite nanocubes and the size of Ag nanoparticles can significantly affect the activity and selectivity of CO_2 photoreduction to CO/CH_4. This novel phenomenon was explored and elucidated with the aid of various characterization techniques and the corresponding mechanism reported previously [15,16,32].

2. Experimental

2.1. Material preparation

Brookite TiO_2 is prepared according to our previous report [34]. Typically, 2.85 g (~15 mmol) $TiCl_4$ was dropped into 40 g ice water. After the ice melted, 5.0 g urea was added with continually stirring. Immediately following the urea dispersed, 5.0 mL sodium lactate solution (~60%) was added dropwise, and then the mixture was transferred into a 100 mL Teflon-lined autoclave, which was sealed and kept at 200 °C for 20 h, and then cooled to room temperature naturally. The precipitate was filtered and washed with distilled water and absolute ethanol for several times, and then the product dried at 70 °C was calcined in air for 3 h at 500 °C with a heating rate of 2 °C min^{-1}.

Ag-loading on the brookite TiO_2 is conducted as follows: as-prepared brookite TiO_2 (200 mg) and a certain amount of $AgNO_3$ solution were mixed in 100 mL water, then 0.1 g $NaBH_4$ was added to chemically reduce Ag^+ to Ag^0. After 3 h reaction, the suspension was filtered and washed with water and ethanol for several times, and then dried at 70 °C in vacuum overnight to obtain the Ag-loaded product (Ag–TiO_2). All chemical reagents used are of analytical grade and used as received without further purification.

2.2. Material characterization

X-ray powder diffraction (XRD) pattern was obtained by Miniflex 600 X-ray diffractometer with Cu Kα irradiation (λ = 0.154 nm) at 40 kV and 15 mA. A scan rate of 4° min^{-1} was applied to record the XRD patterns in the range of $10° \leq 2\theta \leq 50°$ with a step of 0.02°. The morphology was investigated with Zeiss–Sigma field emission scanning electron microscope (FESEM). The high-resolution transmission electron microscopy (HRTEM) observation was conducted on a LaB_6 JEM-2100(HR) electron microscope (JEOL Ltd.) working at 200 kV.

UV–vis diffuse reflectance absorption spectra (DRS) were obtained by a Shimadzu UV-3600 spectrophotometer equipped with an integrating sphere with $BaSO_4$ as the reference. The scan region is 800 to 200 nm with a step of 1 nm. Time-resolved photoluminescence (PL) spectra were recorded by a Multifunction steady state and transient state fluorescence spectrometer (FES920, Edinburgh Instruments) at 398 nm with 330 nm excitation. X-ray photoelectron spectroscopy (XPS) measurement was performed on a Bruker D8 X-ray photoelectron spectroscope equipped with a standard and monochromatic source (AlKα) operated at 300 W.

In situ diffuse reflectance infrared Fourier transform spectra (DRIFTS) were recorded on a Nicolet iS50 spectrometer (Thermo Electron) equipped with a liquid nitrogen cooled HgCdTe (MCT/A) detector. The spectra in absorbance units, and acquired with a resolution of 4 cm^{-1} by using 256 scans. Typically, 40 mg catalyst was uniformly dispersed onto the DRIFTS accessory, which was then thoroughly vacuum-treated to remove air completely. Then CO_2 (99.999%) gas and H_2O vapour was introduced into the reactor until 1 atm and then maintained for 20 min before collecting IR spectra. CO_2 temperature programmed desorption (CO_2-TPD) curve was determined by using Micromeritics Autochem 2. The sample was firstly heated to 50 °C in flowing Ar for 30 min, and then heated to 800 °C at a heating rate of 10 °C min^{-1} under Ar flowing.

For obtaining the photocurrent and electrochemical impedance spectra (EIS) spectra, a working electrode (Pt wire) was immersed in 50 mL aqueous suspension containing catalyst (25 mg), NaOH (1.9 g) and methyl viologen (6 mg), and a saturated Ag/AgCl electrode and a Pt gauze electrode were used as a reference and a counter electrode, respectively. Before irradiation, the suspension was continuously purged by N_2 to remove O_2, and then illuminated by light from a 300 W Xe-lamp. The working electrode was held at +0.5 V *vs.* Ag/AgCl by using a CHI618 workstation to collect the photocurrent-time curve.

2.3. Photocatalytic activity measurement

CO_2 photoreduction was carried out in a home-made gas-closed circulation system operated under a 300 W Xe-lamp irradiation. In the CO_2 photoreduction system, 0.15 g catalyst was uniformly dispersed onto the watch-glass with an area of ~28 cm^2, which then put in the reaction cell (Pyrex glass) with a total volume of 500 mL. Before irradiation, the above system was thoroughly vacuum-treated to completely remove air. CO_2 and H_2O vapor were produced from the reaction of $NaHCO_3$ (1.00 g, introduced into the reactor before being sealed) and H_2SO_4 solution (5.0 mL, 4 M), which was introduced into the reactor *via* a syringe. During irradiation, 2 mL gas was taken from the reactor at regular intervals (1 h) for subsequent gas concentration analysis using a gas

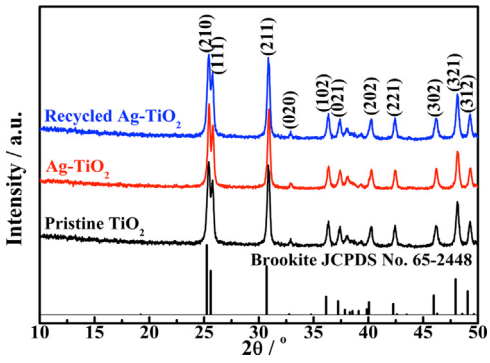

Fig. 1. XRD patterns of the pristine brookite TiO_2, 5.0% Ag–TiO_2 and its recycled product after the CO_2 photoreduction reaction for 20 h.

chromatograph (SP-7820, TDX-01 column, Rainbow chemical instrument Co., Ltd) equipped with a flame ionized detector (FID) and methanizer. The produced gases were calibrated with a standard gas mixture and their identity determined using the retention time.

3. Results and discussion

3.1. Structure and morphology

XRD pattern shown in Fig. 1 depicts that the obtained product is well conformed to the orthorhombic brookite TiO_2 (JCPDS No. 65-2448). The diffraction peaks at 2θ = 25.3, 25.7, 30.8, 32.9, 36.2, 37.3, 40.1, 42.4, 46.0, 48.0, and 49.1° can be attributed to the reflection of (2 1 0), (1 1 1), (2 1 1), (0 2 0), (1 0 2), (0 2 1), (2 0 2), (2 2 1), (3 0 2), (3 2 1), and (3 1 2) planes, respectively. No diffraction peak for any other TiO_2 crystal phase can be detected in the XRD pattern, indicating the synthesized brookite has high phase purity, which is in well agreement with our previous reports [33,34]. Moreover, no reflection peak attributable to Ag or Ag_2O can be observed from the XRD pattern of the 5.0% Ag-loaded product, possibly due to the relatively low content and well dispersity of Ag nanoparticles on the brookite particles [35].

FESEM images (Fig. 2) indicate that most of the brookite particles have quasi nanocube-like morphology and smooth surfaces, which have relatively uniform particle sizes in the range of 15–84 nm with a mean particle size of ~50 nm and occasionally smaller irregular particles loaded on those nanocubes' surfaces (Fig. S1). After the Ag-loading process, those nanocube-like morphology can be maintained, and some smaller bright points can be observed on those nanocubes' surfaces (Fig. 2B–F), which are related to the loaded Ag nanoparticles. Less smaller bright points are observed from Fig. 2B and C at ≤0.5% Ag-loading level, while Ag nanoparticles with an average size of ~10 nm are uniformly dispersed on the brookite nanocubes when the Ag-loading level reaches 1.0% (Fig. 2D). With further enhancing the Ag-loading level, numerous bright points spread on the brookite nanocubes' surfaces (Fig. 2E and F). Especially for 5.0% Ag–TiO_2, many nanocubes are surrounded by Ag nanoparticles even with some Ag nanoparticles dissociated from those nanocubes (Fig. 2F).

The above observations and detailed information can be further confirmed by the TEM images shown in Fig. 3. The brookite nanocubes (Fig. 3A) have relatively smooth surfaces and sharp edges, in accordance with the above FESEM observation. Those uniform perspective projections of discrete nanoparticles indicate that the nanocube-like shape is a complete particle but not an aggregate of small primary particles. The lattice fringes of HRTEM images (inserted in Fig. 3B and C) and their corresponding fast Fourier transform (FFT) patterns indicate that the quasi nanocube is mainly shaped by two (2 1 0) and two $(2\,\bar{1}\,0)$ exposed facets. The interfacial angle between (2 1 0) and $(2\,\bar{1}\,0)$ facets (Fig. 3B, E and H) agrees well with the theoretical calculated value (~80°), and the top and bottom sides of the nanocube are perpendicular to the incident beam (parallel to [0 0 1] direction), indicating the top and bottom sides of the nanocube probably can be assigned to the (0 0 1) facets of brookite. Therefore, it can be concluded that each nanocube is parallel hexahedron which is mainly surrounded by four {2 1 0} and two {0 0 1} exposed crystal facets, and the interfaces of contiguous crystal facets are fairly smooth, which is very similar to the nanosheets reported previously [32].

By carefully examining those lattice fringes and FFT patterns inserted in those HRTEM images, it can be found that the metallic Ag nanoparticles with relatively uniform size (~10 nm) are mainly loaded on the {2 1 0} facets of the 0.5% Ag-loaded brookite nanocubes (Fig. 3D–F), indicating that the Ag^+ ions can be preferentially adsorbed on the exposed {2 1 0} facets of the brookite nanocubes. While for the 5.0% Ag-loaded product, Ag nanoparticles with much broader particle size distribution (10–30 nm) are spread on each exposed facets of the brookite nanocubes (Fig. 3G) and excess Ag nanocrystals can also be observed (marked as circles

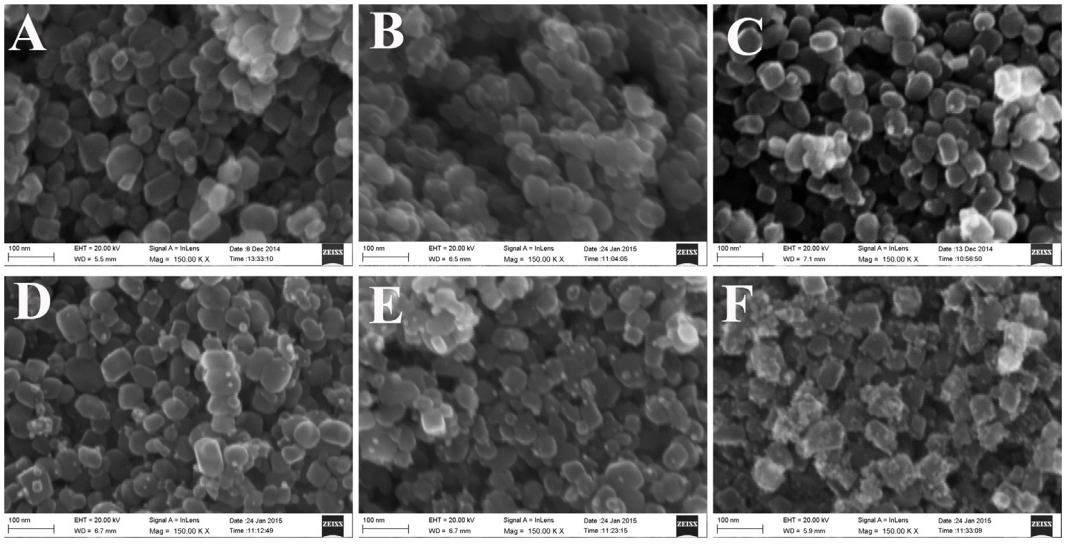

Fig. 2. FESEM images of the pristine brookite TiO_2 (A), 0.1% Ag–TiO_2 (B), 0.5% A–TiO_2 (C), 1.0% Ag–TiO_2 (D), 2.0% Ag–TiO_2 (E), and 5.0% Ag–TiO_2 (F).

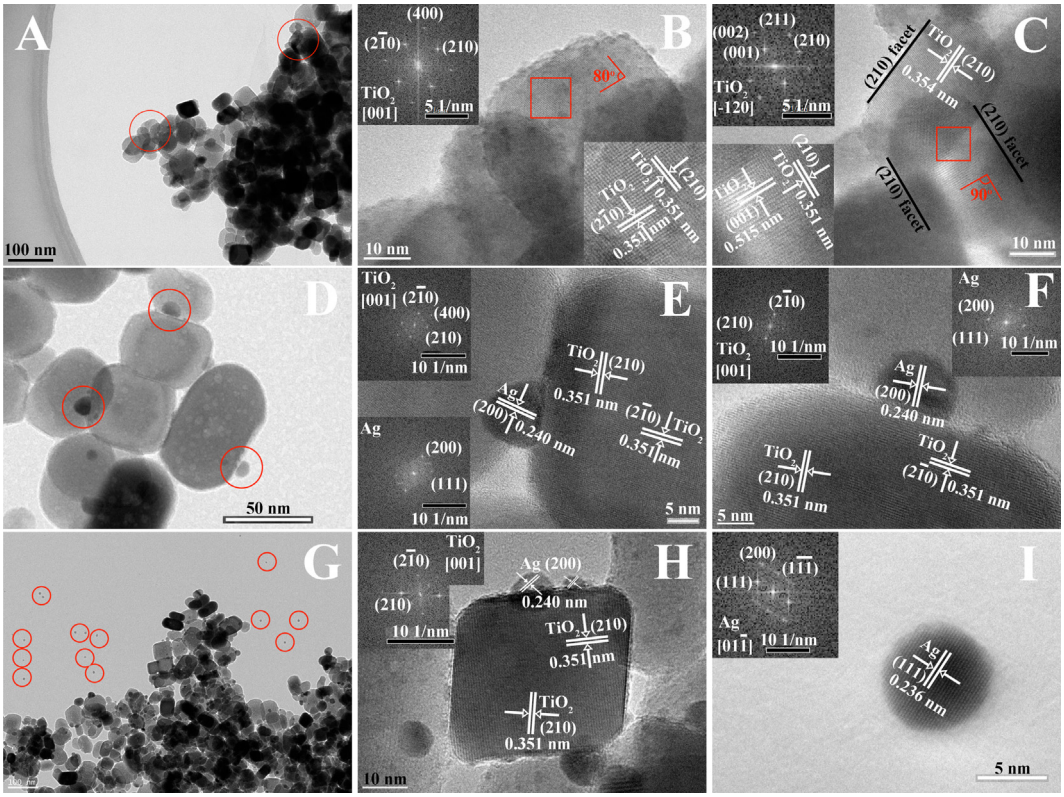

Fig. 3. TEM and HRTEM images of the brookite TiO_2 (A–C) and its Ag-loaded products (0.5% Ag–TiO_2 (D–F) and 5.0% Ag–TiO_2 (G–I)).

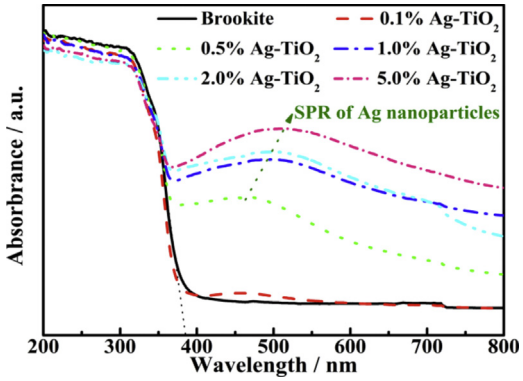

Fig. 4. DRS spectra of the brookite TiO_2 nanocubes and its Ag-loaded products with different loading levels.

in Fig. 3G), possibly due to the non-uniform adsorption of the excessive Ag^+ ions on the nanocubes during the Ag-loading process. Meanwhile, the lattice fringes and FFT patterns of Ag nanoparticles are also matched with metallic Ag (Fig. 3H and I). Furthermore, some dissociative Ag nanoparticles with high crystallinity are formed in the 5.0% Ag–TiO_2 (Fig. 3G–I). It has reported that Ag or Au nanoparticles have notably surface plasma resonance (SPR) effect, which can slightly extend the absorption edge to visible region [35–37]. As can be seen from the UV–vis diffuse reflectance spectra (DRS, Fig. 4), the significant enhancement in absorbance at ~510 nm can be ascribed to the SPR effect of more Ag nanoparticles formed due to the excessive Ag-loading [35]. Moreover, the maximum absorption wavelength of Ag nanoparticles' SPR absorption shifts from ~450 to 510 nm upon enhancing the Ag-loading level (Fig. 4), implying that the Ag nanoparticle size on the brookite can be changed with the Ag-loading level. Therefore, it can be concluded that those Ag nanoparticle's size and distribution on the exposed facets of the brookite nanocubes can be adjusted by changing the Ag-loading level, which would influence the activity and selectivity of CO_2 photoreduction reaction as discussed below.

3.2. Photocatalytic activity and selectivity

Control experiments showed no appreciable reduced C1/C2 product detected in the absence of either catalyst or irradiation, implying that both catalyst and irradiation are necessary for the present gaseous CO_2 photoreduction system. The primary results showed CO_2 can be selectively reduced to CO and CH_4 in the presence of H_2O vapor and the brookite nanocubes (or its Ag-loaded products), and no other reduced product such as CH_3OH, HCHO or HCOOH is detected in gas or liquid phase by using GC-FID method. Moreover, neither CO/CH_4 nor other carbon-containing organic compounds can be detected when the photoreaction system was introduced N_2 instead of CO_2, demonstrating that the CO/CH_4 generation was stemmed from the CO_2 photoreduction process over the catalyst.

Fig. 5A shows the effects of the Ag-loading level on the CO/CH_4 generation activities of CO_2 photoreduction over the brookite nanocubes during the initial 2 h irradiation. The corresponding overall activity for the CO/CH_4 generation can be estimated with total consumed electron number (TCEN), which is calculated with Eq. (1).

$$\mathrm{TCEN} = \frac{2 \times (c_{\mathrm{CO}} + 4c_{\mathrm{CH_4}}) \times V_{\mathrm{reactor}}}{m_{\mathrm{cat.}} \times t_{\mathrm{irr.}}} \quad (1)$$

where TCEN is the total consumed electron number for the CO/CH_4 generation. V_{reactor} is the reactor volume. $t_{\mathrm{irr.}}$ is the irradiation time. $m_{\mathrm{cat.}}$ is the catalyst mass. c_{CO} and $c_{\mathrm{CH_4}}$ are the produced CO and CH_4 concentration, respectively.

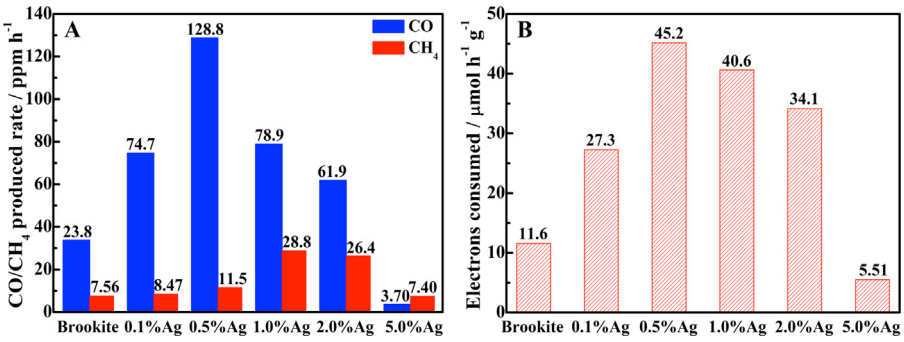

Fig. 5. Effects of the Ag-loading level on the CO/CH_4 production rate (A) and the total consumed electron number (B) for the CO_2 photoreduction over the brookite TiO_2 nanocubes during the initial 2 h light irradiation.

The pristine brookite shows relatively low generation activity of 23.8 (CO) and 7.56 (CH_4) ppm h^{-1} with CO/CH_4 molar ratio of 3.15 (Fig. 5A). CO generation activity shows an obvious increasing trend when the Ag-loading level is enhanced from 0 to 0.5%, and then goes downhill with further enhancing the Ag-loading level though the CH_4 generation activity shows a gently increasing one until the Ag-loading level is 1.0%. Especially, 0.5% Ag–TiO_2 shows a maximum CO generation activity (128.8 ppm h^{-1}), which is 5.41 times higher than that (23.8 ppm h^{-1}) of the pristine one; while the 1.0% Ag–TiO_2 exhibits a maximum CH_4 generation activity (28.8 ppm h^{-1}), which is only 3.80 times higher than that (7.56 μmol h^{-1} g^{-1}) of the pristine one. The overall activity for the CO/CH_4 generation over the present brookite nanocubes can be estimated with the TCEN value shown in Fig. 5B. Namely, 0.5% Ag–TiO_2 shows an optimal overall activity with TCEN value as high as 45.2 μmol h^{-1} g^{-1}, which is 3.89 times higher than that (11.6 μmol h^{-1} g^{-1}) of the pristine one. As-mentioned above, helium pretreatment of brookite TiO_2 resulted in the creation of surface V_O and Ti^{3+} sites, which can leads to an enhanced photoactivity for the CO_2 photoreduction to CO/CH_4 [32]. Possibly, the better photoactivity of the present Ag-loaded products than the pristine one can be also ascribed to the similar reason because the brookite nanocubes are treated with $NaBH_4$ solution during the Ag-loading process. Therefore, the photoactivity of the brookite after treated by $NaBH_4$ solution without addition $AgNO_3$ solution is also conducted, and the corresponding results are shown in Fig. S2. As can be seen, the brookite after treated with $NaBH_4$ solution without Ag-loaded also shows low production activity of 25.3 (CO) and 9.09 (CH_4) ppm h^{-1}, which is similar to the pristine one as shown in Fig. 5A. It means that the treatment with $NaBH_4$ solution cannot significantly affect the photoactivity of the pristine brookite. Hence, the enhanced photoactivities of the Ag-loaded products are not attributed to the treatment with $NaBH_4$ solution, but the Ag-loading levels and its distributions on the brookite nanocubes.

The selectivity for the CO generation can be evaluated by the produced CO/CH_4 molar ratio shown in Fig. 6. CO/CH_4 molar ratio gets a peak at 0.5% Ag-loading and then significantly reduces upon further enhancing the Ag-loading level to 1.0%. Nevertheless, the overall activity (TCEN value) only shows a limited decrease when the Ag-loading level is enhanced to 1.0% and 2.0% (Fig. 5B). This implies that 0.5% Ag-loading is more beneficial for the CO generation from the present CO_2 photoreduction process, while slightly higher Ag-loading level is propitious to selective CH_4 production though 5.0% Ag–TiO_2 shows a very low overall activity. Since the Ag-loading level affects not only the particle size and its distribution on the exposed facets of the brookite nanocubes, but also the Ag/TiO_2 nanoparticles' interfacial structure as mentioned above, the changing trends of activity and selectivity for the CO/CH_4 generation dependent on the Ag-loading level can be related to the synergistic effects of Ag/TiO_2 interfaces, Ag nanoparticle size and its distribution on the nanocubes' exposed facets, which would influence the light harvesting, charge recombination and even CO_2/H_2O adsorption.

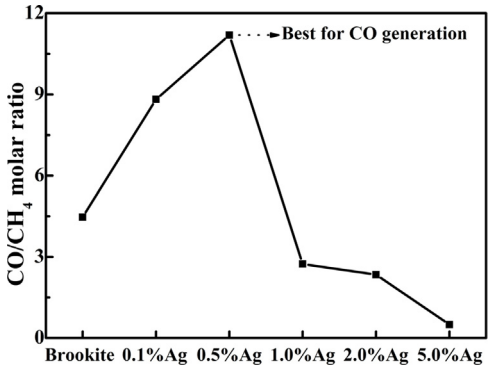

Fig. 6. Effect of Ag-loading level on the produced CO/CH_4 molar ratio over the brookite TiO_2 nanocubes.

Although the mechanism of CO_2 photoreduction to solar fuels is complex and the detail information is not well understood up till now [38–42], it is a consensus that the H^+ from H_2O and the adsorption states of carbonates (or its hydrolytes) serve as the important intermediates of the CO_2 photoreduction reaction. Possibly, the products are CO/CH_4 gas rather than CH_3OH, HCHO, HCOOH or other carbohydrates can be ascribed to the less H^+ concentration in the present gaseous system [40–42]. Hence, *in situ* DRIFT spectra are measured so as to further comprehend the relationship between the Ag nanoparticle's size/distribution on the exposed facets and the activity/selectivity of the present CO_2 photoreduction to CO/CH_4 generation. As shown in Fig. 7A, the pristine brookite and its Ag-loaded products show similar IR peaks at ~3726 cm^{-1} and 3691–3703 cm^{-1} ascribable to the surface hydroxyl groups (such as Ti^{3+}–OH and Ti^{4+}–OH), indicating the adsorption of hydroxyl group is not affected by Ag-loading [43,44]. Therefore, the activity/selectivity of the present CO_2 photoreduction might be mainly related to the differences of carbonates (or its hydrolytes) adsorption stemmed from various Ag-loading levels.

The pristine brookite shows IR peaks at ~1300/1426 cm^{-1} ascribable to the dissociative CO_2 (Fig. 7B) [32,45], while those peaks cannot be be observed from those Ag-loaded products. It proves that the pristine brookite has poor CO_2 adsorption capability, which may be the reason that the activity for CO_2 photoreduction over the pristine brookite is very limited as shown in Fig. 5. After Ag-loading, monodentate carbonate (m-CO_3^{2-}), bidentate carbonate (b-CO_3^{2-}) and bicarbonate (HCO_3^-) are formed on the brookite surfaces (Fig. 7B) [16,32,45], suggesting that the Ag nanoparticles on the brookite are benefit to adsorb carbonates

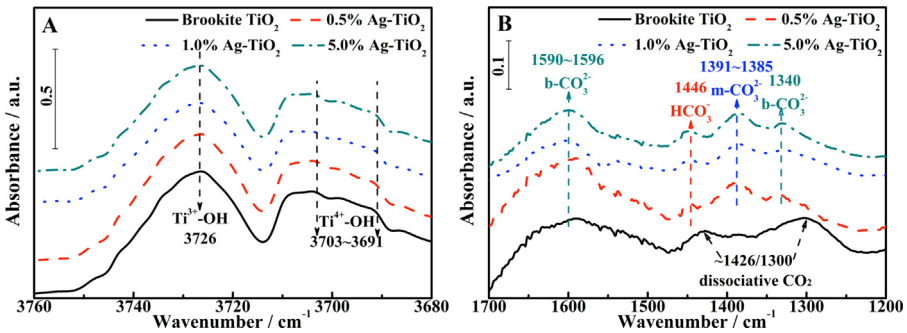

Fig. 7. *In situ* DRIFTS IR spectra of H_2O (A) or CO_2 (B) interaction with the brookite TiO_2 nanocubes or its 0.5%, 1.0% and 5.0% Ag-loaded products.

and/or its hydrolytes. CO_2-TPD curves also show that almost no obvious peak around 300–750 °C can be observed from the pristine brookite (Fig. S3A), indicating the poor CO_2 adsorption capability of the pristine brookite, while Ag-loading can significantly enhance the CO_2 adsorption capacities with changed adsorption states (Fig. S3B–F). For example, at Ag-loading level ≤0.5%, CO_2–TPD curves show slightly enhanced peak around 300–450 °C (Fig. S3B and C), indicating the increased physical adsorption capability of CO_2 on the brookite, while >0.5% Ag-loaded products show obvious peak around 550–750 °C except for the enhanced peaks around 300–450 °C (Fig. S3D–F), implying higher Ag-loading level would lead to the increased physical/chemical adsorption of CO_2. Furthermore, there is an obvious peak centered at ~520 °C as observed from the CO_2–TPD curve (Fig. S3F) of 5.0% Ag-TiO_2, which cannot be observed in the lower Ag-loading levels. Since the TEM images (Fig. 3G and H) for 5.0% Ag-TiO_2 shows that some dissociative Ag nanoparticles are well dispersed, the CO_2–TPD peak at ~520 °C might be related to the CO_2 adsorption on those dissociative Ag nanoparticles. Obviously, this CO_2 adsorption on the dissociative Ag nanoparticles would compete with those on the brookite nanocubes.

Generally, the Ag nanoparticles with a proper loading level on the brookite nanocubes can not only serve as electron sink by formation of Schottky junctions at the semiconductor/metal interfaces to promote the photogenerated carrier separation in space [35,46], but also act as activated sites for the CO_2 photoreduction [38]. On the one hand, the loaded Ag nanoparticles can serve as electron sink at the semiconductor/metal interfaces [46], which benefits to separate the photoinduced carriers in space. It can be validated from the time-resolved PL spectra shown in Fig. S4. The electron lifetime (τ_2) is slightly extended from 3.56 ns (the pristine one) to 4.28 ns by 0.5% Ag-loading, indicating the enhanced charge separation efficiency. At ≤0.5% Ag-loading levels, Ag nanoparticles are almost dispersed on the {2 1 0} facets of the brookite nanocubes as mentioned above (Fig. 3). It implies that the photoinduced electrons would be mainly dispersed on the {2 1 0} facets of the brookite nanocubes. Possibly, those electrons mainly dispersed on the {2 1 0} facets of the brookite nanocubes would result in the higher activity for CO generation. On the other hand, the m-CO_3^{2-} and b-CO_3^{2-} adsorption capacities are more significantly increased as compared to HCO_3^- for the 0.5% Ag-loading (Fig. 7B). It is well matched the selectivity of CO generation for the 0.5% Ag–TiO_2. Hence, it can be conjectured that the highest CO generation activity at 0.5% Ag-loading can be related to the Ag nanoparticles dispersed on the {2 1 0} facets of the brookite nanocubes, which leads to the suitable carrier separation and CO_3^{2-} adsorption.

With enhancing the Ag-loading level higher than 0.5%, the {2 1 0} facets of the brookite nanocubes might be completely occupied, and Ag nanoparticles trend to aggregate on the {2 1 0} facets (Fig. 2D–F) and even load on the {0 0 1} facets (Fig. 3G and I). The IR peak at 1446 cm^{-1}, corresponding to the HCO_3^- adsorption [16,32],

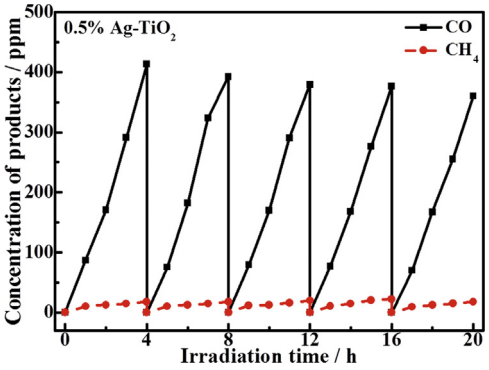

Fig. 8. Typical time course for CO and CH_4 generation over the 0.5% Ag-loaded brookite TiO_2 nanocubes under 300 W Xe-lamp irradiation.

become more obvious as compared with 0.5% Ag–TiO_2 (Fig. 7B). This enhancement of HCO_3^- adsorption of 1.0% Ag–TiO_2 should be related to the additional Ag-loading on the {0 0 1} facets of the brookite nanocubes. Moreover, the CO_2–TPD curves (Fig. S3D and E) show that the CO_2 adsorption amounts are increasing as well. A wide peak at around 300–400 °C can be observed, which can be attributed to the CO_2 desorption from HCO_3^- adsorbed on the weak basic sites [47–49]. Therefore, the selectivity of CH_4 generation at 1.0% and 2.0% Ag-loading levels can be ascribed to the efficient HCO_3^- adsorption on the brookite. Perhaps, those enhanced HCO_3^- adsorption is related to the additional Ag nanoparticles loaded on the {0 0 1} facets of the brookite nanocubes as mentioned above. Meanwhile, the electron lifetime (τ_2 4.86 ns) of 1.0% Ag-loading is also longer than the other catalysts (Fig. S4), implying that a more efficient carrier separation causes the relatively high CO/CH_4 generation activity.

As the Ag-loading amount reaches 5.0%, Ag nanoparticles tend to aggregate on the brookite surface and form dissociative nanoparticles (Fig. 3G–I), which would lead to decreased light harvesting efficiency of the brookite. Also, those aggregated Ag nanoparticles would become the charge recombination centers, which results in a significant decrease in the electron lifetime (2.13 ns) (Fig. S4), while those dissociative Ag nanoparticles would compete in the CO_2 adsorption (Fig. S3F), which leads to the decreased adsorption of reactants on brookite. Therefore, the harmful CO_2 adsorption, the inefficient charge separation and light harvesting lead to the significantly decreased activity of the 5.0% Ag–TiO_2.

3.3. Photocatalytic stability

Fig. 8 depicts the typical time course for CO and CH_4 generation over the 0.5% Ag–TiO_2, which are investigated in five consecutive runs of accumulatively 20 h with refreshed CO_2 periodically replaced in each run. No noticeable decrease in the

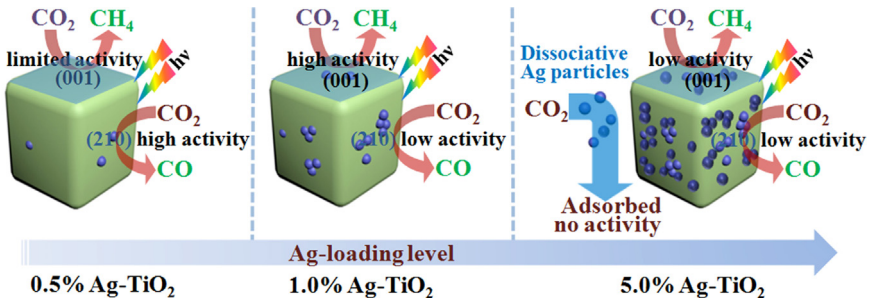

Fig. 9. Possible influencing mechanism of the Ag-loading level on the activity and selectivity of CO_2 photoreduction to CO/CH_4 generation.

activity/selectivity for the CO/CH_4 generation (with 95% activity maintained) can be found for the present catalyst after 20 h irradiation. Since the reaction of CO_2 photoreduction for CH_4 production is involving 8 electrons transfer, which is more complex than the reaction for the CO production with 2 electrons transfer [38–42], and the protons concentration for water vapor is very limited in the present gas phase condition, the reaction of CO_2 photoreduction for the CH_4 production is easily affected by the reaction condition as compared with the reaction for the CO production, and hence the decrease of CH_4 production rate is more obvious than CO at each run as shown in Fig. 8.

XRD pattern (Fig. 1) of the recycled 0.5% Ag–TiO_2 after 20 h irradiation shows no obvious deviation in these main diffraction peaks as compared with the original one, indicating the stable crystal structure of the brookite TiO_2. XPS spectra (Fig. S5) of 0.5% Ag–TiO_2 and its recycled one also indicate that the survey spectra have no deviation for the locations of the main elements (Fig. S5A). Moreover, both of the high resolution XPS spectra (Fig. S5B) of Ti2p for 0.5% Ag–TiO_2 and its recycled one have similar doublet peaks at 464.1 and 458.3 eV with a binding energy gap of 5.8 eV, which conforms to Ti^{4+} $2p_{1/2}$ and $2p_{3/2}$ orbits of brookite [35], indicating the stable electron structure of the brookite nanocubes' exposed facets.

Nevertheless, a slight drop in the activity of CO_2 photoreduction can still be observed during recycling runs even exchanging fresh CO_2 as shown in Fig. 8. It can be concluded that some metallic Ag near the surface may be oxidized to form Ag^+ by those photoinduced holes and/or photooxidant, which can result in the deactivation [35]. As shown in Fig. S5C, the XPS spectra of Ag3d orbit is asymmetry and can be decomposed into two peaks. One strong peak at 367.2 eV with a splitting energy of 6.0 eV, which are related to metallic Ag $3d_{3/2}$ and $3d_{5/2}$; the other weak one at 368.0 eV with a splitting energy of 6.0 eV can be related to monovalent Ag^+ $3d_{3/2}$ and $3d_{5/2}$. The weak Ag^+ signals in the fresh Ag–TiO_2 indicate metallic Ag can easily transform to monovalent Ag^+ in air [35,46]. After 20 h irradiation, the XPS peak (at 368.0 eV) related to Ag^+ increases slightly, which is well matched the deactivation in activity (Fig. 8). Although the spectra of O1s (Fig. S5D) seem to change a lot in shape after irradiation, the positions of XPS peaks remain at the binding energies of 531.6 and 529.8 eV, which can be related to the hydroxyl adsorbed on the surface and Ti-O bonds in brookite TiO_2, respectively [15,16,35]. The significant increase of hydroxyl peak can be ascribed to the hydroxyl adsorption on the brookite during the photoreaction process.

3.4. Discussion on enhanced activity and selectivity mechanism

Combining with the above discussion on Ag nanoparticle size/distribution (Figs. 2 and 3) and CO_2 adsorption states (Fig. 7 and Fig. S3) dependant on the Ag-loading level, a proposed mechanism for the enhanced activity and unique selectivity over the present Ag-loaded brookite nanocubes is shown in Fig. 9. Under irradiation, photogenerated electrons are excited from the valence band (VB) to the conduction band (CB) of the brookite with positive holes left in the VB. It is generally agreed that cocatalysts serve as electron sink by formation of Schottky junctions at the semiconductor/metal interfaces, and the cocatalyst with larger work function should more readily trap electrons [46]. As reported previously, Ag is not a good cocatalyst for H_2 evolution, but benefit to CO evolution over Ag loaded catalyst or Ag modified electrode [50]. It can be related to the much weaker binding energy of CO on Ag surface so that CO can frequently leave the catalyst surface and refresh the active sites for the subsequent reduction reaction [50].

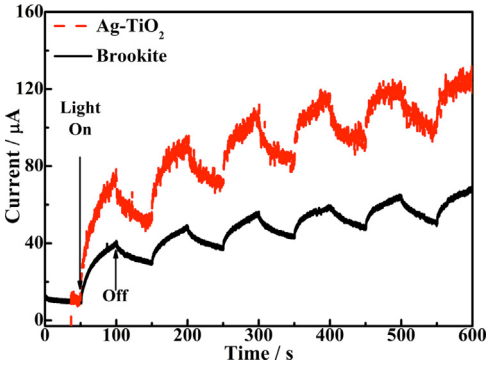

Fig. 10. Typical photocurrent-time curves of the brookite TiO_2 nanocubes or its 0.5% Ag-loaded product in NaOH solution suspension under light irradiation.

As shown in Fig. 9, at low Ag-loading level (for example, 0.5%), the selectivity for the CO generation might be due to the Ag nanoparticles uniformly dispersed on the exposed {2 1 0} facets of brookite nanocubes. As shown in Fig. 10, the photocurrent response of 0.5% Ag–TiO_2 is stronger than the pristine one, which can be ascribed to a more efficient charge separation by trapping electrons of the loaded Ag nanoparticles. The enhancement in CH_4 generation selectivity for 1.0% and 2.0% Ag–TiO_2 is mainly related to the additional Ag nanoparticles loaded on the {0 0 1} facets, which provides the activated sites for the chemical adsorption of CO_2 (Fig. S3D–F) and more sites for the HCO_3^- adsorption (Fig. 7B) [32,45–49]. The stable HCO_3^- adsorptions provide opportunities to the reaction of carbon and hydrogen intermediate to form CH_4. While the decrease in overall activity in high Ag-loading level (for example, 5.0%), which would lead to Ag nanoparticles aggregation and dissociative Ag nanoparticles, and causing the negative effects in light harvesting, charge recombination and the competitions in CO_2/H_2O adsorption, and then the significantly decreased activity.

The effects of Ag-loading levels on the charge recombination process can be further validated from the EIS spectra (see Supporting information, Fig. S6 and Table S1, for details). The R_2 in the simple simulated equivalent circuit represents the impedance in medium and low frequency of the photocatalyst suspension [33,34], which changes significantly in dark and light irradiation. Under irradiation, the dramatically decreases in the resistance is due to the efficient charge separation (Table S1). The pristine brookite only shows ~44% R_2 decrease ratio, while those Ag-loaded products have a R_2 decrease ratio up to ~70%, and R_2 is decreasing with the enhancement of Ag-loading levels, which is attributed to a better electronic conductivity of metallic Ag. It's in a well agreement of the above proposed mechanism that the photointroduced electrons transferred from TiO_2's CB to the loaded Ag nanoparticles. Especially for 0.5% Ag–TiO_2, the R_2 decrease ratio is the maximum (~77%) among the tested catalysts, which is corresponding to the best overall activity (Fig. 5). The significant decrease of R_2 value is observed from the 1.0% and 2.0% Ag-loaded products as compared with 0.5% Ag-loaded one, which coincides with the change of CO_2–TPD curves (Fig. S3C–E). It is evidence that Ag nanoparticles loaded on the other facets such as the {0 0 1} facets are the benefit to the charge transfer and complex reactions, which provide the enhancement in the CH_4 generation activity. Moreover, the electron lifetime (τ_n) can be determined by the position of the low frequency peak (less than 100 Hz) in the Bode plots (Fig. S6) through the equation that $\tau_n = 1/(2\pi f)$, where f means the frequency of superimposed AC voltage. As can be seen from Table S1, the decrease ratios in the electron lifetime for those products with ≥1.0% Ag-loaded levels are ~60% under irradiation. It is due to the high activity of those loaded Ag nanoparticles on the nanocube surfaces, which are benefit to the electron transfer from catalyst to the adsorbed CO_2 and protons, and then enhance the photoactivity especially for the more complex reaction for the CO_2 photoreduction to CH_4. Hence, the great changes in the electron lifetime (τ_n) of 1.0% and 2.0% Ag-loaded products under irradiation (Table S1) also conform the efficient charge transfer and selective CH_4 generation as mentioned above.

4. Conclusion

In conclusion, brookite TiO_2 quasi nanocubes (mean size of ~50 nm) mainly surrounded by four {2 1 0} and two {0 0 1} exposed facets were used as catalyst for the CO_2 photoreduction. Ag nanoparticles with different particle size and distribution on the exposed facets of the brookite nanocubes were successfully synthesized by changing the Ag-loading level during an $AgNO_3$ chemical reduction process. Those Ag nanoparticle size and its distribution on the exposed facets of the brookite nanocubes significantly influence the activity and selectivity of CO_2 photoreduction to CO/CH_4 generation. 0.5% Ag–TiO_2 shows a maximum CO generation activity (128.8 ppm h^{-1}), which is 5.41 times higher than that (23.8 ppm h^{-1}) of the pristine one; while the 1.0% Ag–TiO_2 exhibits a maximum CH_4 production activity (28.8 ppm h^{-1}), which is only 3.80 times higher than that (7.56 μmol h^{-1} g^{-1}) of the pristine one. When the Ag-loading level is ≤0.5%, the small Ag nanoparticles are mainly dispersed on the {2 1 0} facets of the brookite nanocubes, which resulting in an enhancement in the selective CO generation; while 1.0% Ag-loading could lead to the formation of large Ag nanoparticles aggregrated on the {2 1 0} facets with some Ag nanoparticles dispersed on the {0 0 1} facets, and then causing more selectivity for the CH_4 generation. The present results on the activity and selectivity for the CO/CH_4 generation dependent on the Ag-loading level can be related to the charge transfers, adsorption properties and light harvesting synergistically, and providing an important indication about the effects of Ag-loading on the CO_2 photo-reduction performance of brookite TiO_2, which fulfills the deficiency of the research on the photocatalytic CO_2 reduction activity of brookite TiO_2.

Acknowledgements

This work was supported by the Natural Science Foundation of China (21271146, 21171134, 20973128, and 20871096), the Funds for Creative Research Groups of Hubei Province (2014CFA007) and the Fundamental Research Funds for the Central Universities (2042014kf0228) of China.

Appendix A. Supplementary data

Supplementary data associated with this article can be found, in the online version, at http://dx.doi.org/10.1016/j.apcatb.2015.06.022

References

[1] J. Mao, K. Li, T.Y. Peng, Catal. Sci. Technol. 3 (2013) 2481–2498.
[2] A. Goeppert, M. Czaun, J.P. Jones, G.K. Surya Prakash, G.A. Olah, Chem. Soc. Rev. 43 (2014) 7995–8048.
[3] E.V. Kondratenko, G. Mul, J. Baltrusaitis, G.O. Larrazabal, J. Perez-Ramirez, Energy Environ. Sci. 6 (2013) 3112–3135.
[4] F. Fresno, R. Portela, S. Suarez, J.M. Coronado, J. Mater. Chem. A 2 (2014) 2863–2884.
[5] A. Cybula, M. Klein, A. Zaleska, Appl. Catal. B: Environ. 164 (2015) 433–442.
[6] T. Jin, C. Liu, G.H. Li, Chem. Commun. 50 (2014) 6221–6224.
[7] Y. Kou, Y. Nabetani, D. Masui, T. Shimoda, S. Takagi, H. Tachibana, H. Inoue, J. Am. Chem. Soc. 136 (2014) 6021–6030.
[8] Y. Kou, S. Nakatani, G. Sunagawa, Y. Tachikawa, D. Masui, T. Shimada, S. Takagi, D.A. Tryk, Y. Nabetani, H. Tachibana, H. Inoue, J. Catal. 310 (2014) 57–66.
[9] Y.S. Liao, S.W. Cao, Y.P. Yuan, Q. Gu, Z.Y. Zhang, C. Xue, Chem.-A Eur. J. 20 (2014) 10220–10222.
[10] E.G. Ha, J.A. Chang, S.M. Byun, C. Pac, D.M. Jang, J. Park, S.O. Kang, Chem. Commun. 50 (2014) 4462–4464.
[11] J.G. Yu, J. Jin, B. Cheng, M. Jaroniec, J. Mater. Chem. A 2 (2014) 3407–3416.
[12] W. Kim, T. Seok, W. Choi, Energy Environ. Sci. 5 (2012) 6066–6070.
[13] R.X. Zhou, M.I. Guzman, J. Phys. Chem. C 118 (2014) 11649–11656.
[14] G.X. Song, F. Xin, J.S. Chen, X.H. Yin, Appl. Catal. A: Gen. 473 (2014) 90–95.
[15] J. Mao, T.Y. Peng, X.H. Zhang, K. Li, L. Zan, Catal. Commun. 28 (2012) 38–41.
[16] J. Mao, L.Q. Ye, K. Li, X.H. Zhang, J.Y. Liu, T.Y. Peng, L. Zan, Appl. Catal. B-Environ. 144 (2014) 855–862.
[17] L.Q. Ye, J. Mao, T.Y. Peng, L. Zan, Y.X. Zhang, Phys. Chem. Chem. Phys. 16 (2014) 15675–15680.
[18] J. Mao, T.Y. Peng, X.H. Zhang, K. Li, L.Q. Ye, L. Zan, Catal. Sci. Technol. 3 (2013) 1253–1260.
[19] M.M. Gui, S.P. Chai, B.Q. Xu, A.R. Mohamed, Sol. Energy Mater. Sol. Cells 122 (2014) 183–189.
[20] H.C. Hsu, I. Shown, H.Y. Wei, Y.C. Chang, H.Y. Du, Y.G. Lin, C.A. Tseng, C.H. Wang, L.C. Chen, Y.C. Lin, K.H. Chen, Nanoscale 5 (2013) 262–268.
[21] N.M. Dimitrijevic, B.K. Vijayan, O.G. Poluektov, T. Rajh, K.A. Gray, H.Y. He, P. Zapol, J. Am. Chem. Soc. 133 (2011) 3964–3971.
[22] J.G. Yu, J.X. Lou, W. Xiao, P. Zhou, M. Jaroniec, J. Am. Chem. Soc. 136 (2014) 8339–8342.
[23] M. Tahir, N.A.S. Amin, Appl. Catal. B: Environ. 162 (2015) 98–109.
[24] X. Li, J.Q. Wen, J.X. Low, Y.P. Fang, J.G. Yu, Sci. China Mater. 57 (2014) 70–100.
[25] S. Rani, N.Z. Bao, S.C. Roy, Appl. Surf. Sci. 289 (2014) 203–208.
[26] I. Tanabe, T. Ryoki, Y. Ozaki, Phys. Chem. Chem. Phys. 16 (2014) 7749–7753.
[27] K. Fan, T.Y. Peng, J.N. Chen, X.H. Zhang, R.J. Li, J. Power Sources 222 (2013) 38–44.
[28] M.M. Rodriguez, X. Peng, L. Liu, Y. Li, J.M. Andino, J. Phys. Chem. C 116 (2012) 19755–19764.
[29] W.K. Li, X.Q. Gong, G. Lu, A. Selloni, J. Phys. Chem. C 112 (2008) 6594–6596.
[30] H. Lin, L. Li, M. Zhao, X. Huang, X. Chen, G. Li, R. Yu, J. Am. Chem. Soc. 134 (2012) 8328–8331.
[31] T. Ohno, T. Higo, N. Murakami, H. Saito, Q. Zhang, Y. Yang, T. Tsubota, Appl. Catal. B: Environ. 152–153 (2014) 309–316.
[32] L.J. Liu, H.L. Zhao, J.M. Andino, Y. Li, ACS Catal. 2 (2012) 1817–1828.
[33] K. Li, J.L. Xu, W.Y. Shi, Y.B. Wang, T.Y. Peng, J. Mater. Chem. A 2 (2014) 1886–1896.
[34] J.L. Xu, K. Li, S.F. Wu, W.Y. Shi, T.Y. Peng, J. Mater. Chem. A 3 (2015) 7453–7462.
[35] Z. Jiang, Q. Ouyang, B.S. Peng, Y.X. Zhang, L. Zan, J. Mater. Chem. A 2 (2014) 19861–19866.
[36] R.G. Li, F.X. Zhang, D.G. Wang, J.X. Yang, M.R. Li, J. Zhu, X. Zhou, H.X. Han, C. Li, Nat. Commun. 4 (2013) 1432.
[37] J.X. He, P.J. Yang, H. Sato, Y. Umemura, A. Yamagishi, J. Electroanal. Chem. 566 (2004) 227–233.

[38] H. Zhou, P. Li, J.J. Guo, R.Y. Yan, T.X. Fan, D. Zhang, J.H. Ye, Nanoscale 7 (2015) 113–120.
[39] I. Inoue, A. Fujishima, S. Konishi, K. Honda, Nature 277 (1979) 637–638.
[40] M.A. Butler, D.S. Ginley, J. Electrochem. Soc. 125 (1978) 228.
[41] B. Kumar, M. Llorente, J. Froehlich, T. Dang, A. Sathrum, C.P. Kubiak, Annu. Rev. Phys. Chem. 63 (2012) 541–569.
[42] A.A. Peterson, F.A. Pedersen, F. Studt, J. Rossmeisl, J.K. Norskov, Energy Environ. Sci. 3 (2010) 1311–1315.
[43] A. Glisenti, L. Ferretto, Chem. Mater. 15 (2003) 1181–1188.
[44] S.H. Szczepankiewicz, A.J. Colussi, M.R. Hoffmann, J. Phys. Chem. B 104 (2000) 9842–9850.
[45] H.Y. He, P. Zapol, L.A. Curtiss, J. Phys. Chem. C 14 (2010) (2010) 4–21481.
[46] K. Li, A.D. Handoko, M. Khraisheh, J.W. Tang, Nanoscale 6 (2014) 9767–9773.
[47] K. Nomura, Y. Ujihira, T. Hayakawa, K. Takehira, Appl. Catal. A: Gen. 137 (1996) 25–36.
[48] K.M. Merz, J. Am. Chem. Soc. 112 (1990) 7973–7980.
[49] A. Yan, B. Liu, Y. Dong, Z. Tian, D. Wang, M. Cheng, Appl. Catal. B-Environ. 80 (2008) 24–31.
[50] A.A. Peterson, J.K. Nørskov, J. Phys. Chem. Lett. 3 (2012) 251–258.